A quasi-geostrophic diagnosis of the zonal flow associated with cut-off lows over South Africa and surrounding oceans

Thando Ndarana[1,*], Tsholanang S. Rammopo[1], Hector Chikoore[2], Michael A. Barnes[3] and Mary-Jane Bopape[4]

[1]Geography, Geoinformatics and Meteorology, University of Pretoria, Hatfield, South Africa

[2]Unit for Environmental Sciences and Management, North-West University, Vanderbijlpark, South Africa

[3]Marine Research Unit, South African Weather Service, Cape Town, South Africa

[4]Department of Research and Innovation, South African Weather Service, Centurion, South Africa

*Correspondence to Thando Ndarana. Email: thando.ndarana@up.ac.za

Abstract

The zonal flow associated with cut-off lows (COLs) comprises two jet streaks of different spatial extents. The smaller scale jet streak, located north of the COLs, forms as a result of meridional divergence of vorticity advection and it is quasi-stationary, relative to the COLs. It dissipates as the COLs do the same. The larger scale jet streak gives rise to anticyclonic and equatorward Rossby wave breaking (RWB) as it propagates southeasterly to the base of the ridge, south of the COL and then northeasterly beyond that point. As the jet streak propagates it brings with it the anticyclonic barotropic shear that causes the Rossby waves to break. Its propagation is caused by zonal momentum advection by the zonal flow from jet streak entrance to its exit. As it propagates, its northwesterly/southeasterly orientation changes to one that is more zonal to become south-westerly/northeasterly at the end of the COL life cycle. This change in orientation is due to meridional advection of zonal momentum,where the meridional flow advects momentum southward (northward) at the jet streak entrance (exit). The jet streaks form a split jet structure and the winds between the streaks is decelerated by vorticity advection convergence. Because the flow and COL (and RWB) life cycle are coupled, understanding the dynamics that underlie the changes in the COL ambient flow contributes to resolving the outstanding RWB/COL causality problem.

Introduction

Cut-of-low (COL) pressure systems are one of the most important all-seasons (Singleton and Reason 2007) precipitation producing systems over South Africa, with an annual frequency maximum occurring in autumn and a secondary maximum in spring (Singleton and Reason 2007; Pinheiro et al. 2017). During the spring, the rainfall associated with these systems is more intense and widespread (Favre et al. 2013), thus contributing the most to annual COL precipitation. During the winter months COLs can also bring about heavy snowfall, when coupled with low level systems that facilitate cold temperature advection at the surface (Stander et al. 2016). COLs may also occur together with ridging high pressure systems. The latter facilitate the influx of moisture from the Indian Ocean (Dyson 2015; Ndarana et al. 2020) into southern Africa. Under these circumstances COLs may result in flooding and extensive damage to property. There are numerous cases of this particular combination of systems. One example is the devastating 1987 Natal (now KwaZulu-Natal) Province flooding event during which more than 600 mm of rainfall fell within a short period of 4 days. The

damage to property caused by this event was estimated to be in hundreds of millions of USD and a death toll of 380 people having lost their lives (Bell 1995). More recently, from 21-24 April 2019 an equally devastating COL event was reported. It too caused floods and extensive damage to property. During this event over 85 people lost their lives. Therefore an improved understanding of their dynamics may be important for predictability problems over South Africa, particularly at the medium range forecasting time scales, which is important for early warning systems.

Using the vorticity equation, Godoy et al. (2011) showed that the local change of the relative vorticity in COLs is influenced by horizontal vorticity advection, which would serve to cause their eastward propagation (Holton and Hakim 2014), even though they may be quasi-stationary (Abatzoglou 2016). However, the evolution of relative vorticity within COLs does not elucidate the importance and role of the flow around these systems, except perhaps in as far as the vorticity advection is concerned. A more useful perspective in that respect is that of local energetics (Orlanski and Katzfey 1991; Orlanski and Sheldon 1995). COLs are associated with two eddy kinetic energy (EKE) centers; one develops at the base of the closed circulation, whilst another is located first, to the southwest of the circulation (Gan and Piva 2013). The EKE centre within the closed circulation develops by gaining energy from the larger scale structure via ageostrophic geopotential fluxes. The convergence of these fluxes maintain the COLs (Gan and Piva 2016).

The fact the EKE within COLs is imported from an upstream source outside the closed circulation highlights the importance of ambient flow conditions to COL dynamics and evolution. As far back as Price and Vaughan (1993), COLs have been shown to be associated with jet streaks. Jet streaks are upper level frontal wind zones whose dynamics and evolution are influenced by curvature and shear vorticity advection (Martin 2014) and have also been simulated by numerical models (e.g. Singleton and Reason 2006).

In the Northern Hemisphere, the jet streak starts propagating from the western flank of the low. At this point the streak exhibits a north-west/south-east orientation. It then propagates in a south-easterly direction to the base of the trough, and eventually ends up in the eastern inflection point of the trough (Shapiro 1982; Keyser and Shapiro 1986). Some observation studies have presented departures from this conceptual model (e.g. Pyle et al. 2004; Lang and Martin 2012). In these studies it was shown using quasi-geostrophic analysis that there are cases in which the jet streaks are located in the north-westerly and south-westerly flows, without progressing across the trough axis. Even with these differences, these studies have shown that jet streak dynamics play an important role in baroclinic waves. In the Southern Hemisphere (SH), COLs are associated with two jet streaks, one which is larger and initially located south-west of the COL closed circulation and the other located north of the closed circulation (Ndarana and Waugh 2010; Reyers and Shao 2019). The latter is quasi-stationary, whilst the other propagates to the base of the ridge south of the closed circulation of the COL. The ridge is indicated by the low potential vorticity (PV) anomalies (Fig. 6 in Ndarana and Waugh 2010; Fig. 6 in Reyers and Shao 2019).

Because the results of Ndarana and Waugh (2010) and Reyers and Shao (2019) showed that the formation and dissipation of COLs is coupled to the evolution of their ambient zonal flow, understanding the dynamics of this evolution is of particular interest for addressing causality problems associated with COLs. The ambient flow leads to Rossby wave breaking (RWB, Peters and Waugh 2003) or intrusions into the upper troposphere (Waugh and Polvani 2000) and, subsequently, the high PV anomalies that induce the closed COL circulation

(Hoskins et al. 1985). However, the dynamical processes that cause this evolution have not been addressed in the literature as yet. Therefore, the aim of this study is to diagnose and explain the dynamical processes that underlie the development and changes in the jet streaks that are associated with COLs. The remainder of the paper is structured as follows, in Sect. 2 the Data and Methods are presented. The results are provided in Sect. 3, with subsections that include a review of the discussion of the zonal flow that is associated with COLs, the influence of quasi-geostrophic processes on the flow and the impact of advective processes on the zonal flow. In Sect. 4 we give the concluding remarks.

Data and methods

Data

We use 39 years (1979–2018) of European Centre for Medium-Range Weather Forecasting (ECMWF) Reanalysis (ERA-Interim) dataset (Dee et al. 2011) to identify COLs in 500 hPa geopotential height fields, in longitude and latitude. ERA-I employs four dimensional variational (4D-Var) data assimilation, which as far as we know, is one of the most advanced data assimilation methods at present. The ECMWF data assimilation system makes use of the Integrated Forecasting System, which incorporates a model with the fully coupled Earth system comprising of the atmosphere, land surface and ocean waves (Dee et al. 2011). The reanalysis data it produces is therefore considered reliable, but only from 1979 because of the introduction and assimilation of satellite data from that year (Tennant 2004). This is particularly important for the Southern Hemisphere, and Africa in particular, because these regions are data sparse compared to most regions in the Northern Hemisphere. The version of the data used in the study has a 2.5° × 2.5° horizontal grid spacing, which suffices because COLs are synoptic scale processes with a horizontal extent $L \sim 10^6$ m. The time interval at which the data is available is 6-hourly.

Methods

COL detection

The detailed method and steps for identifying COLs is provided in Barnes et al. (2020), only a brief description of it is provided in the current study. This is an eight step method that exploits the ability of MATLAB to identify precise indices in a matrix of data through which a contour of a particular value passes. Ndarana et al. (2018) used a similar approach to identify ridging South Atlantic anticyclones in the South African domain.

First, for each 6 hourly time step, contours of 500 hPa geopotential heights at 10 gpm contour intervals from the minimum to the maximum geopotential height value are obtained. For a contour to be considered closed, the longitudes and latitudes of the beginning and end of it must be exactly the same. The centre of each closed contour is the middle most grid point and these points are saved as potential COL points. In the second step we exclude tropical, subpolar and polar lows as potential COLs by requiring that the latitude and longitudes centres of the closed contours be confined to the 15°– 50 °S latitude ring, following Singleton and Reason (2007).

The first two steps identifies potential closed circulations but do not distinguish between high and low pressure systems. To do this, in the third step we further require that the geopotential

height value at each potential COL point be lower than the values of the 6 surrounding grid points by a minimum of 10 gpm (Nieto et al. 2005; Rebeita et al. 2006). The fourth step ensures that the closed contours comprise a cyclonic circulation that is detached from the westerly wind belt and we additionally require that the zonal component of flow south of the potential COL point be negative.

COLs have a cold core (Pelmén and Newton 1969). As in Ndarana and Waugh (2010), we use the 850–500 hPa thickness fields to separate potential COL points that comply with the cold core condition from those that do not. A COL point is considered to be associated with a cold core of the close cyclonic circulation if its thickness value is lower than that of at least five of the surrounding grid points surrounding it. All the COL points that do not comply with this requirement are then filtered out. This constitutes the fifth step of the algorithm.

In the sixth step, concentric closed contours are then grouped together and considered to characterise the same COL pressure system. This is done by requiring that COL points that belong to the same COL be within a 10° x 10° grid box. The final COL point is the centroid with the lowest 500 hPa geopotential height and all the other COL points are discarded. A subjective inspection of the COL points revealed that some COL pressure systems have missing time steps in between. Porcù et al. (2007) observed a similar problem in their study. This is a problem that materialises in 6 hourly data because in studies that employed daily data (Ndarana and Waugh 2010; Reboita et al. 2010) it did not happen. A COL was deemed to have a gap if there were no more than two consecutive missing 6-hourly detections. Gaps in the COL were filled with a closed contour, low pressure minima point database. This database was created as with the COL database, but without applying zonal wind or cold core conditions. A gap was filled by a low-pressure minimum point within a $5^{\circ} \times 5^{\circ}$ degree box of the previous COL point if it existed.

In the eighth and final step, we determine the evolution of the COLs. To do this, we employ the distance which a COL is likely to travel within a 6 h period. Because COLs are synoptic systems, their time scale is $L/U \sim 10^5$ s. This translates to the fact that 6 h these systems are likely to travel less than 1000 km, assuming that $U \sim 10$ m s^2 (Holton and Hakim 2014). Using this criterion, all consecutive COL points that occur within a 1000 km radius comprise a single system. After implementing these steps, we found that the maximum distance between any two consecutive COL points is less than 1000 km and is 165 km on average. From this the duration of COLs is then determined. Only cases that develop and dissipate east of 60°W and 50°E were considered for this study to cover South Africa and surrounding oceans.

Composite analysis

We first calculate all the fields that will be used in the analysis. These are both components of the geostrophic flow, the absolute vorticity advection and its meridional divergence, the Eulerian acceleration of the zonal geostrophic flow as well as the advection terms in the zonal quasi-geostrophic momentum equation. These diagnostics involve the calculation of derivatives, which are evaluated by means of second order finite differencing. Using the centre of the COLs determined by the methods described above i.e. (ϕ_c,λ_c), as the reference point, we formulate composite fields of all the variables in the following manner:

- For each variable, a subset of the data bounded by (ϕ_c−22.5∘,λ_c−50°), (ϕ_c−22.5∘,λ_c+50°), (ϕ_c+22.5∘,λ_c+50°) and (ϕ_c+22.5∘,λ_c−50°) is extracted from the SH fields.
- The subset fields are then brought together, so that the (ϕ_c,λ_c) coincide. This essentially brings all the geopotential heights and other variables into phase. The fields are then averaged and the evolving composite fields are produced as functions of relative latitude, relative longitude and time.

In the following two sections we discuss the various dynamical processes that are involved in informing the evolution of the zonal flow. In all the figures, the 95% level statistical significance of the composite fields is represented by the areas with crosses. It was calculated using Brown and Hall (1999).

Results

The zonal flow and potential vorticity associated with COLs

Whilst the focus of this study is not the variability of COLs, but the flow associated with them, it is of interest to note that the intra-annual variation profile of the COL events in the domain covering South Africa and surrounding oceans (bounded by 60°W and 50°) is similar to that in Fuenzalida et al. (2005), Favre et al. (2013) and Ndarana and Waugh (2010) on the 500 hPa level. This is shown by the dotted red curve in Fig. 1a. COLs that actually enter the region bounded by 10°E and 40° as in Singleton and Reason (2007) show the well known April maximum and secondary but lower maxima in August and October (dashed dotted black curve in Fig. 1a). These profiles give credence to the algorithm presented in the previous section. In addition the frequency of COLs decreases exponentially as a function of duration. This is consistent with other synoptic weather systems such as ridging high pressure systems (e.g. Ndarana et al. 2018) that are important for rainfall in the South African domain.

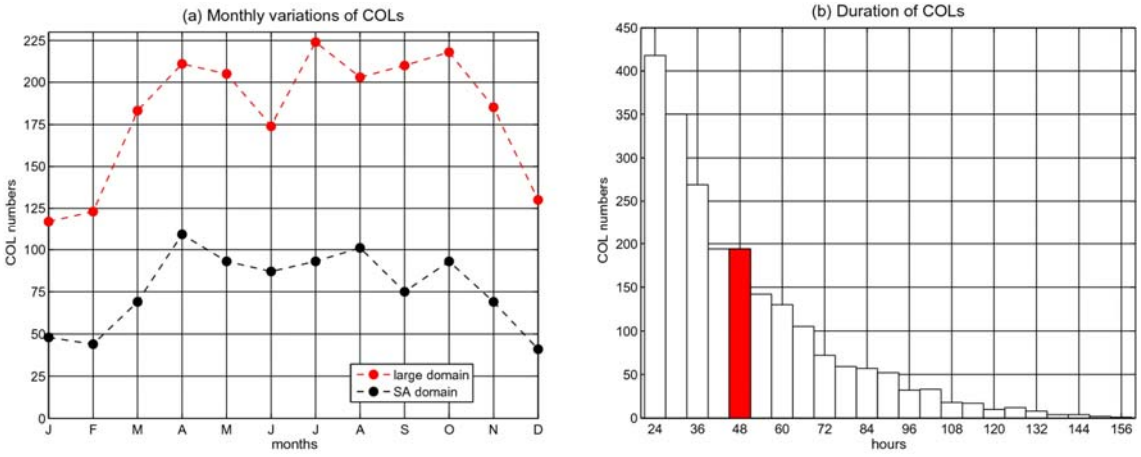

Fig. 1. Frequency of cut-off lows as a function of **a** months and **b** duration. The duration of the cut-off lows is provided in 6 h intervals in **b**. The red curve in **a** represents frequency COLs in the larger domain and the black one represents COLs that actually enter the smaller domain bounded by 10°E and 40°E

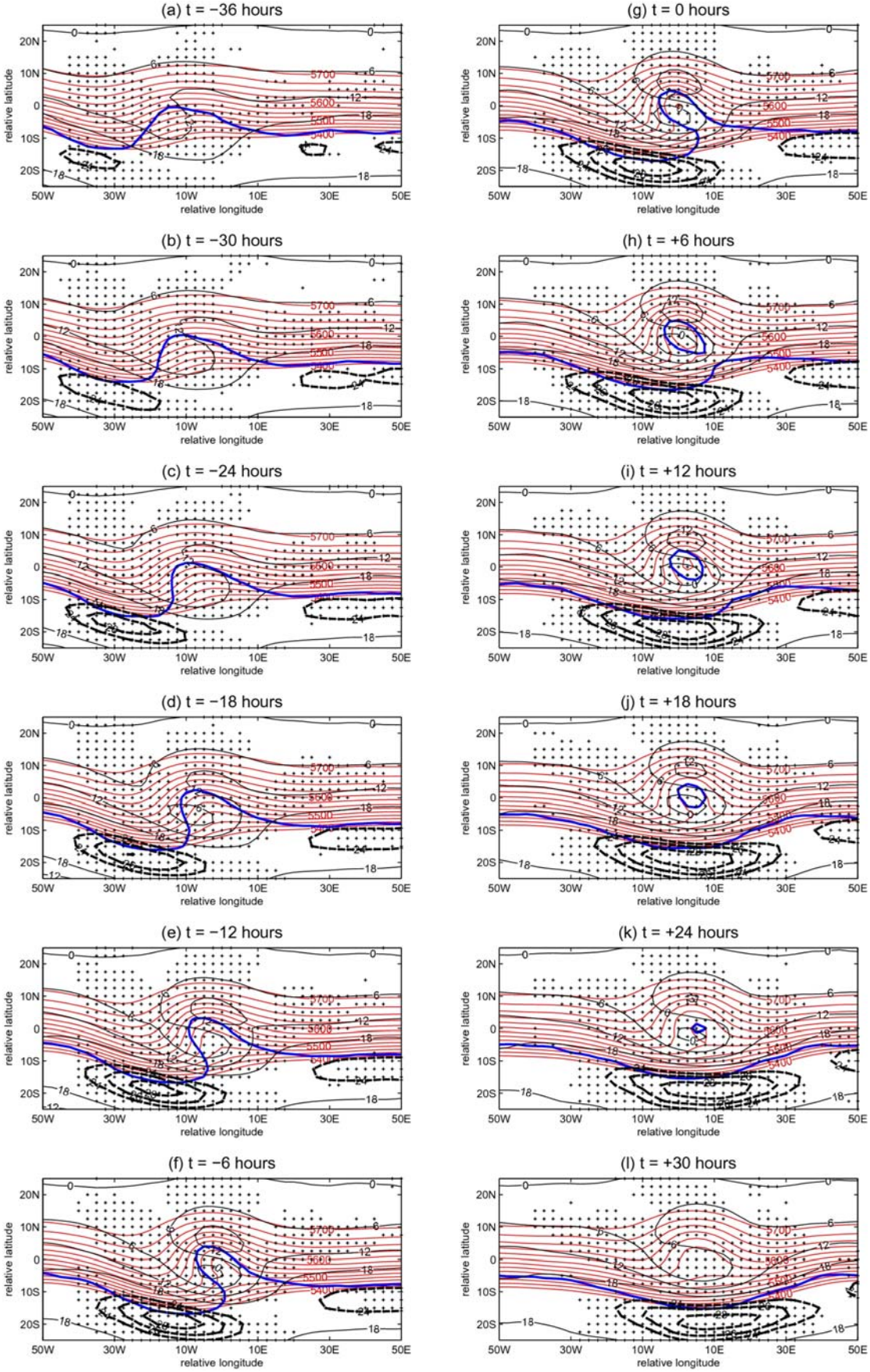
(a) t = −36 hours
(g) t = 0 hours
(b) t = −30 hours
(h) t = +6 hours
(c) t = −24 hours
(i) t = +12 hours
(d) t = −18 hours
(j) t = +18 hours
(e) t = −12 hours
(k) t = +24 hours
(f) t = −6 hours
(l) t = +30 hours
relative latitude
relative longitude
20N
10N
0
10S
20S
50W
30W
10W
10E
30E
50E
5700
5600
5500
5400

Fig. 2. Time-lagged composites of 500 hPa geopotential heights (red contours), zonal component of the 500 hPa geostrophic wind (black contours with thick dashed contours highlighting the jet streak) and – 3 PVU contour (thick blue contour) on the 330 K isentropic surface. The zonal geostrophic isotachs are plotted in 6 m s^{-1}. The jet streaks are highlighted by the thick black dashed contours are plotted in 2 ms−1. The crosses represent areas in the composite where the zonal wind anomalies ($\delta u_g = u_g - \bar{u}_g$, where $\bar{u}_g$ is the seasonal cycle) are statistically significant at the 95% level. The COLs included in this composite calculation have a 48 h duration (red bar in Fig 1 b). The composites are plotted from **a** t = − 36 h to **l** t = +30 h, plotted in 6 h intervals

We now consider the general evolution characteristics of the zonal flow that is associated with COLs using the composite means of all COLs that have a 48 h duration (red bar in Fig. 1b), but the results are similar for events of other durations. Figure 2 shows these composites, and a total of 194 cases were involved in their calculation. Before the formation of the COLs, the progression of events begins with a broken jet structure (Fig. 2a), similar to that observed by Peters and Waugh (2003) and Bowley et al. (2019). This jet is located in the midlatitudes as indicated by its relative latitude to that of the COL position. As the COLs form at t = 0 h (Fig. 2g), they are located between one smaller jet streak to their north and a larger one to their south (highlighted by the thick black dashed contours and may be referred to here as the midlatitude jet streak). The small scale jet streak forms, reaches maximum strength as the COLs develop and become deeper. It dissipates as the COLs do the same. This small scale jet streak is largely quasi-stationary, relative to the COLs. The larger one propagates as the geopotential heights evolve, and it reaches the south of the closed circulation after having propagated south eastward in the north-westerly flow. This movement of the jet streak causes a split jet to form. It eventually passes the COL region where its orientation is most zonal (t = + 24 h Fig. 2k) during its evolution, and ends up downstream of where the closed circulation was located before it dissipated. The evolution of the midlatitude jet streak resembles the north-westerly flow case in Lang and Martin (2012), see their Fig. 5a. The difference is that in our case, the jet streak changes direction at the base of the ridge, in stead of the trough.

The zonal flow anomalies, obtained by removing the seasonal cycle were also superimposed on the zonal geostrophic isotachs in Fig. 2. The structure of the two fields and their evolution are exactly the same (not shown). This suggests that analysis of the total flow and that of the anomalies are equivalent. The 95% statistical significance level of the anomalies represented by the crosses in Fig. 2, together with the Ndarana and Waugh (2010) result obtained using a different reanalysis and that of Reyers and Shao (2019) that focused on a different region in the Southern Hemisphere, suggest that the formation and evolution of the jet streak and split jet are a robust feature of zonal flow that is associated with COLs. These features are also independent of season (not shown).

The broken jet structure and its associated barotropic shear, give rise to RWB (Peters and Waugh 2003; Bowley et al. 2019) because of increasing strain rates (Nakamura and Plumb 1994) which is informed by the increasing strength of the jet streak. This is indicated by the potential vorticity (PV) contour overturning (the behaviour of the thick blue contour in Fig. 2) that manifests from about 24 h before the formation of the COLs. The waves break in an anticyclonic direction, with a thin tongue of high PV air extending equatorward, and then breaking off to form a high PV anomaly; exactly where the closed circulation forms. This is the equatorward and anticyclonic wave breaking (LC1) that is seen in many idealised modelling studies of baroclinic life cycles (e.g. Thorncroft et al. 1993; Kunz et al. 2009; Wang and Polvani 2011; Kunkel et al. 2016). Since the calculations of the composites presented in Fig. 2 do not make any assumptions about PV overturning, and as it appears automatically in the way that it does, they suggest that most of the COLs are associated with

wave breaking and that the wave breaking process precedes COL formation. This strengthens the hypothesis that equatorward anticyclonic RWB events are a necessary precondition for COLs to form (Ndarana and Waugh 2010), because the PV anomalies that result from them induce the cyclonic circulation (Hoskins et al. 1985) that characterises the COLs. It also gives credence to the state of the art for objectively identifying COLs in long datasets (Pinheiro et al. 2017, 2019) that include the existence of a high PV anomaly as an additional criterion.

It follows then that since the ambient flow conditions influence the RWB type that develops and eventually leading to COLs, the former is also necessary for COLs to form. This emphasizes the importance of understanding the dynamical processes that give rise to this zonal flow structure. Even though the flow fields shown in Fig. 2 are geostrophic, they are very similar to those discussed in Ndarana and Waugh (2010) and Reyers and Shao (2019). Therefore, the processes that inform the formation of the configurations and their evolution that were established in those studies can be explained by means of the quasi-geostrophic framework.

Influence of quasi-geostrophic processes on the flow

The fact that u_g shown in Fig. 2 evolves means that its changes may be explained by examining the Eulerian acceleration field, $\partial_t u_g$. To calculate the latter at time t and at each grid point (ϕ,λ), we use the velocity field at t + 6 h and t – 6 h. Composites of u_g and $\partial_t u_g$, presented in Fig. 3, show that there is increasing deceleration of the zonal flow leading up to the formation of the COLs, in the vicinity of the closed circulation. Dong and Colucci (2015) found a similar result for blocking. As would be expected, the small scale jet streak north of this region is also consistent with the Eulerian acceleration field that develops there. There is also a large scale region of $\partial_t u_g > 0$ that has a northwestern/southeastern orientation initially located south west of the closed circulation. It exhibits interesting behaviour from t=0 h as indicated by the highlighted areas using the thick dashed closed white contours. After propagating eastward, the white dashed structure (Fig. 3d at t=0 h) splits into two at t=12 h (Fig. 3e), with the one upstream continuing to propagate in a north easterly direction into the region of the closed COL circulation, and accelerating the flow there. This likely contributes to causing the COL to dissipate, as the zonal wind minimum diminishes there. In addition, examination of the composites in Fig. 3 also shows that there are regions of $\partial_t u_g > 0$ at the exit and east of the midlatitude jet, whilst the confluence region is decelerated. We may then conclude that changes in the zonal flow are informed by the spatial structure of its rate of change. It follows then that processes that inform the Eulerian acceleration, may provide insight into processes that cause the evolution of the flow; including the eastward translation of the midlatitude jet streak.

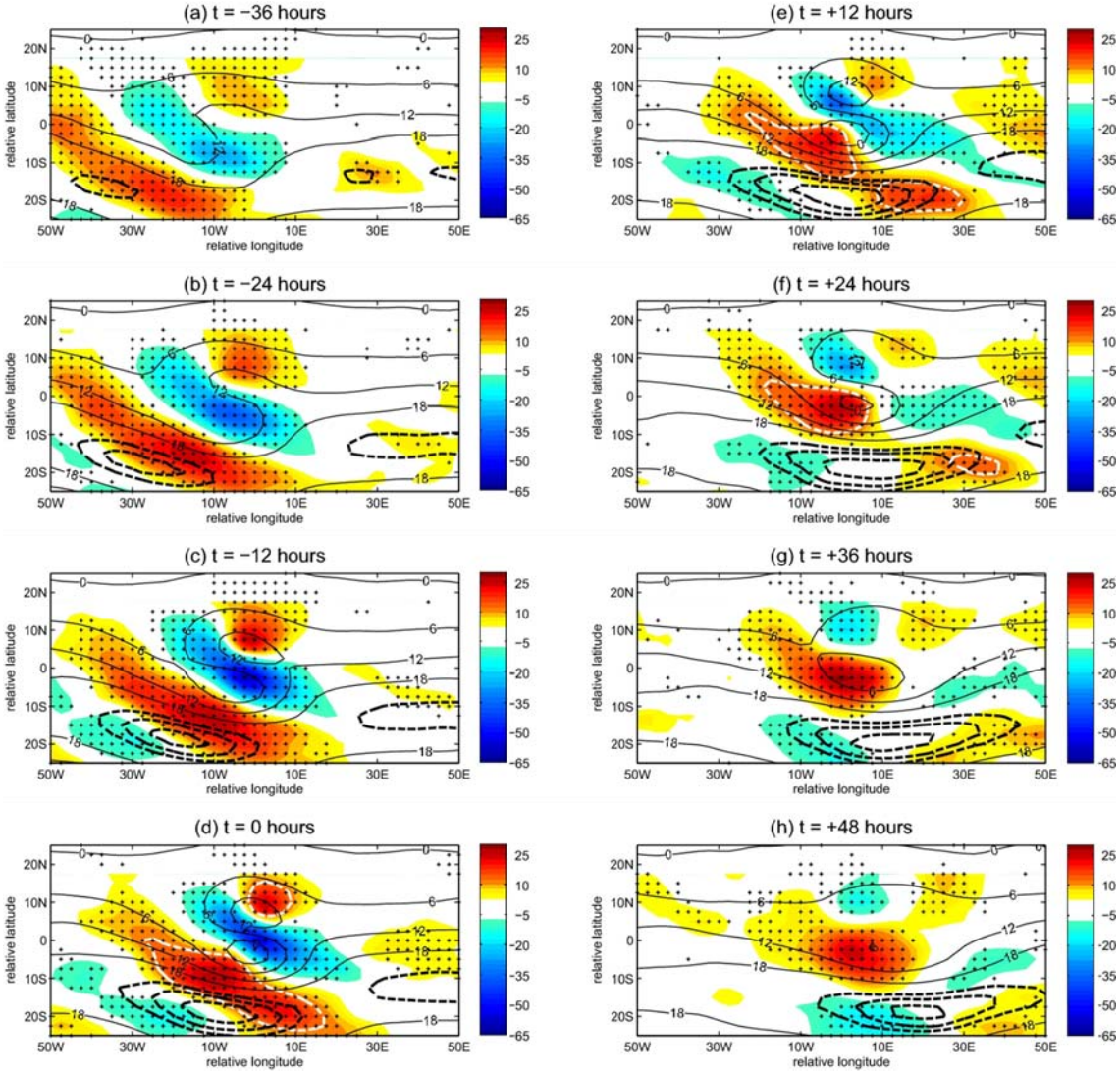

Fig. 3. Time-lagged composites of 500 hPa $\partial_t u_g$ (shaded), plotted in 10^6 m s^{-2}, the thin back contours are as in Fig. 2. The white thick dashed contours represent $\partial_t u_g$=12.5×10^6 m s^2. The crosses represent areas where $\partial_t u_g$ is statistically significant at the 95% level. The composites are plotted from **a** t = –36 h to **l** t = + 30 h, in 12 h intervals

The changes in zonal flow can also be explained by the different stages of the development of the COLs in question. As the low pressure region starts to form and detach from the westerly wind belt, zonal wind speed starts to decelerate. This can be seen in Fig. 3a–d. The westerly belt is "extended" northwards by the protruding COL. This explains the increase in zonal wind speed to the north of the COL. Once a closed low is established (Fig. 3d), an easterly component is established to the south of the core of the COL. Therefore, $\partial_t u_g$ is at a minimum when the closed circulation develops and is at its most mature stage. Once the COL starts to dissipate, the easterly component to the south of the COL starts to decelerate as the closed circulation breaks down and westerly flow is eventually re-introduced. This can be seen to be occurring in Fig. 3e–h.

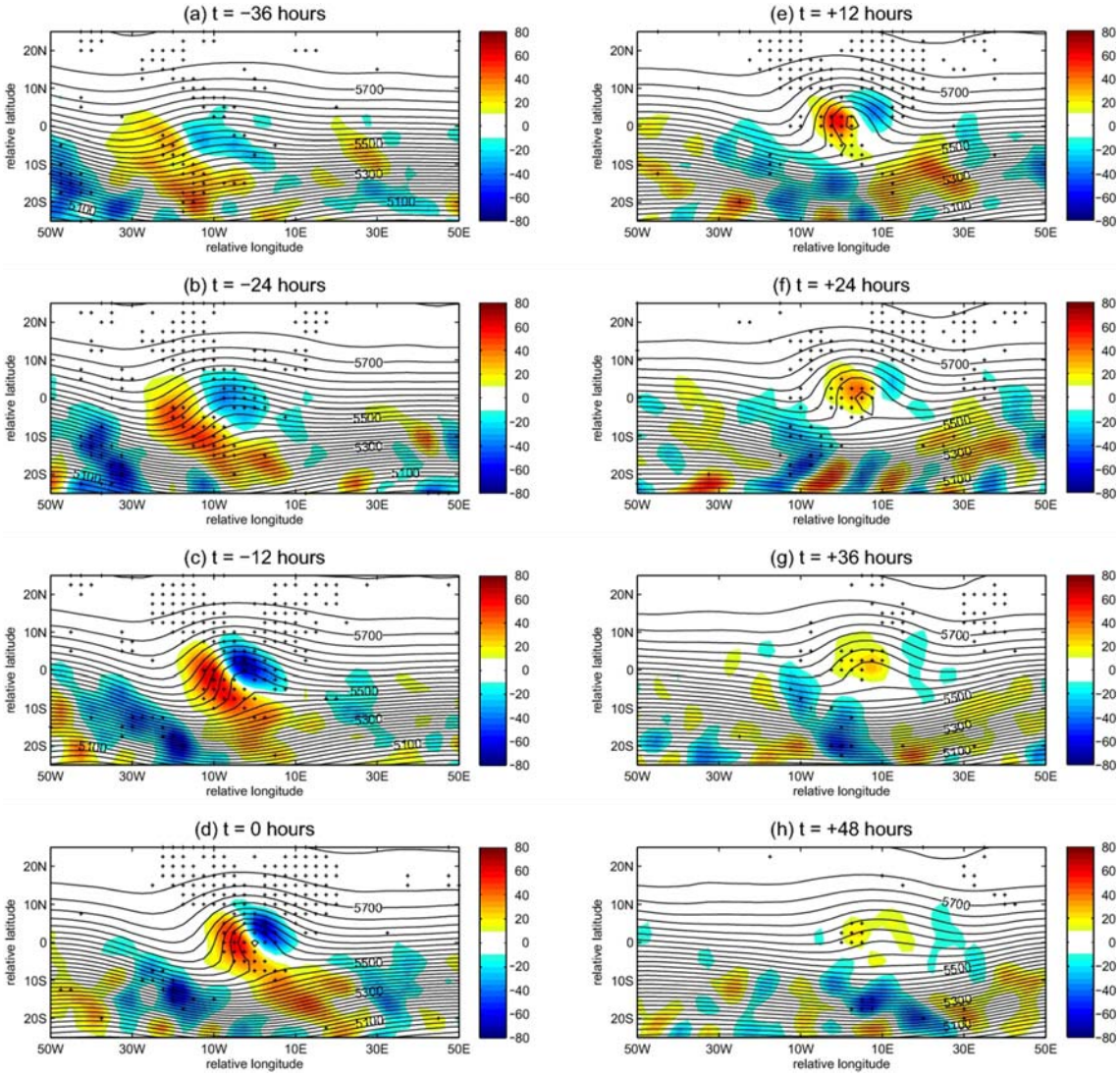

Fig. 4. Time-lagged composites of 500 hPa geopotential heights (black contours), and absolute vorticity advection, $-\mathbf{V}g\cdot\nabla p(\zeta g+f)$, shaded and plotted in 1011 s−2. The crosses represent areas where $-\mathbf{V}g\cdot\nabla p(\zeta g+f)$ is statistically significant at the 95% significance level. The composites are plotted from **a** t = – 36 h to **h** t = + 30 h, in 12 h intervals

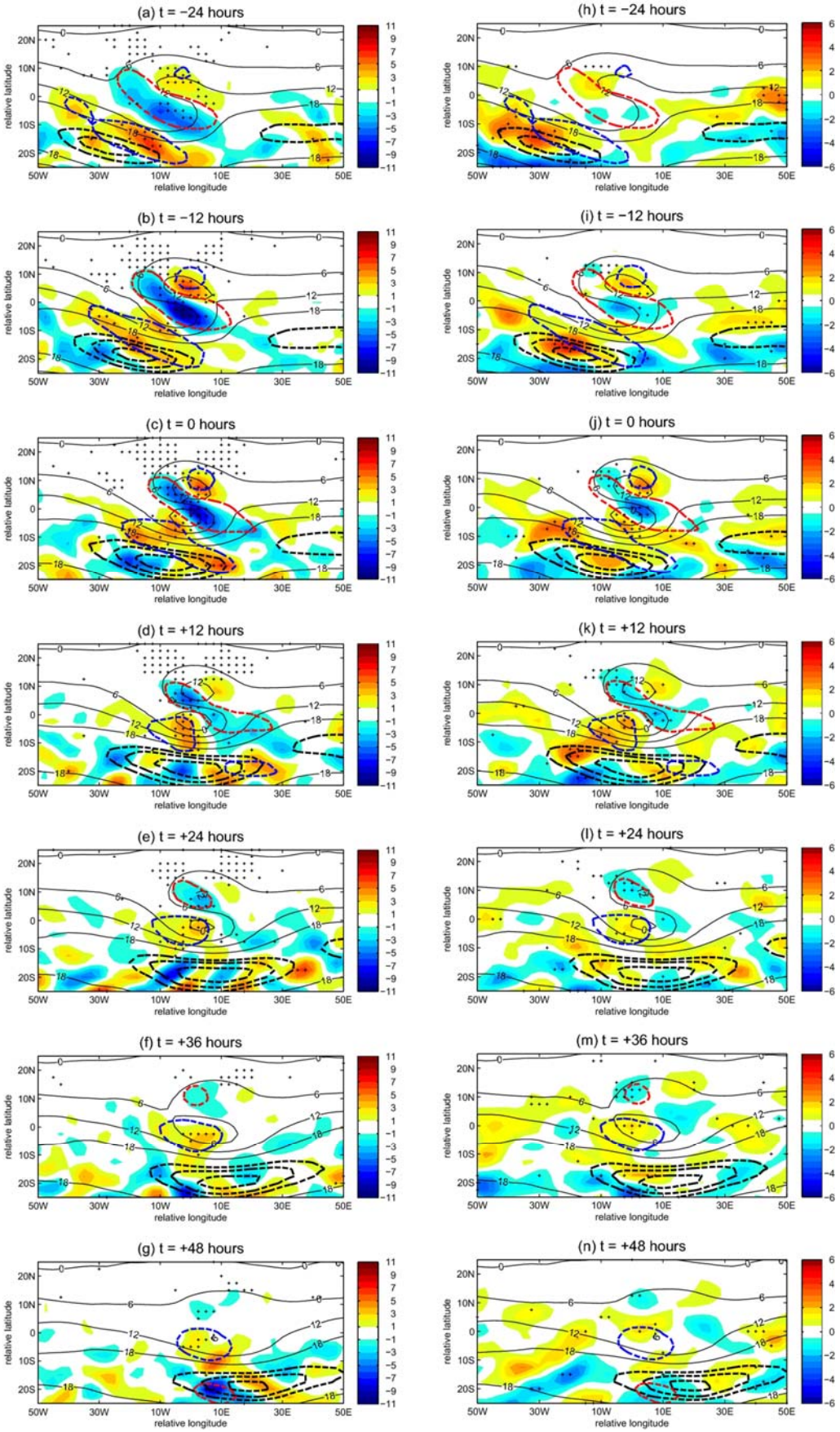
(a) t = −24 hours
(b) t = −12 hours
(c) t = 0 hours
(d) t = +12 hours
(e) t = +24 hours
(f) t = +36 hours
(g) t = +48 hours
(h) t = −24 hours
(i) t = −12 hours
(j) t = 0 hours
(k) t = +12 hours
(l) t = +24 hours
(m) t = +36 hours
(n) t = +48 hours
relative latitude
relative longitude
20N
10N
0
10S
20S
50W
30W
10W
10E
30E
50E

Fig. 5. Time-lagged composites of 500 hPa $\partial y[\mathbf{V}g\cdot\nabla p(\zeta g+f)]$ (vorticity advection divergence—left panels) and $fog\partial y\partial p[(\sigma-1\mathbf{V}g\cdot\nabla p(\partial pz))]$ (temperature advection divergence—right panels), both plotted in 106 m−1 s−2. The black contours are the same as in Fig. 2. The crosses represent areas where the advection fields are significant at the 95% significance level. The composites are plotted from **a, h** t = – 24 h to **g, h** t = + 48 h, in 12 h intervals

To make a case for the use of the quasi-geostrophic framework in diagnosing the zonal flow field, we consider the relationship between the rate of change of geostrophic vorticity (ζ_g, advection of absolute vorticity ($-\mathbf{V}_g\cdot\nabla\eta_g$) and the concentration or dilution of vorticity by the divergence effect ($f_o\partial_p\omega$), where $\mathbf{V}_g=u_g\mathbf{i}+v_g\mathbf{j}$, ω and and f_o are the geostrophic flow, the geostrophic absolute vorticity, the vertical velocity in pressure coordinates, and the Coriolis parameter as at reference latitude (i.e 45◦S), respectively. This relationship is represented as the quasi-geostrophic vorticity prognostic equation (Holton and Hakim 2014). If $U\sim10$ m s−1 and $L\sim10_6$ m are the characteristic scales of horizontal velocity and horizontal extent of COL processes, then the vorticity advection and stretching terms scale as $U2L–2\sim10–10$ s−2 and $U2L–2\sim10–11$ s−2 , respectively. This shows that the two terms differ by an order of magnitude and so we present composites of the former, as the more dominant term. One expects vorticity advection to be positive west of the trough axis and negative east of it. This is clearly the case in Fig. 4 (cf. Fig. 6.8, Holton and Hakim 2014), which is consistent with Godoy et al. (2011), who used ζ instead of ζ_g. Note also that, the trough axis, marked by the curve where the vorticity advection changes sign from positive to negative, has a north-western/south-eastern orientation, indicative of a highly developed system. Where the advection is positive (negative) we also observe positive (negative) relative geostrophic vorticity tendencies (not shown) because of the dominance of this term over temperature advection, as noted above, and also since the latter is stronger at the surface than aloft (Holton and Hakim 2014). Therefore, the rate of change of geostrophic vorticity for COLs is dominated by vorticity advection processes. Whilst COLs can be quasi-stationary (Abatzoglou 2016), there is some evidence of eastward propagation in Fig. 4 which is caused by the dominance of relative vorticity advection over that of planetary vorticity advection since COLs are synoptic scale systems, as predicted by quasi-geostrophic analysis of synoptic scale processes (Holton and Hakim 2014).

The vorticity advection fields behave in a manner consistent with expectations. However, it falls short in explaining the evolution of u_g that is associated with COLs because it is not a forcing on the flow, even though it is a forcing on the geopotential height tendencies (Holton and Hakim 2014). It is its meridional divergence that is and therefore more useful for this purpose. This is clearly seen in the u_g tendency equation, given by

$$\nabla_p^2 + f_o^2\partial_p(\sigma^{-1}\partial_p)]\,\partial_t u_g = \partial_y\,[\mathbf{V}_p\cdot\nabla_p\eta] + f_o g\partial_y\left\{\partial_p\left[\sigma^{-1}\mathbf{V}_g\nabla_p(\partial_p z)\right]\right\} \quad (1)$$

where $\eta=\zeta_g+f$ and the rest of the symbols have been defined above. This equation is obtained by multiplying the geopotential tendency equation by $-(g/f_o)$ and then differentiating the result with respect to y (Dong and Colucci 2015). It can be used qualitatively by recalling that $[\nabla 2p+f2o\partial p(\sigma-1\partial p)]\partial tug\propto-\partial tug$ (Holton and Hakim 2014; Dong and Colucci 2015), to infer the roles that different processes play in changing the zonal flow that is associated with COLs. It follows then, in particular, that $\partial tug\propto\partial y[-\mathbf{V}p\cdot\nabla p\eta]$.

In the vicinity of the COL closed circulation, vorticity advection attains maximum and minimum values at the inflection points of the geopotential heights i.e. where $\partial_x^2 z=0$, and decreases from the inflection axis located west of the COL trough axis to the one located east of it. The immediate implication of this is that $\partial_y[-\mathbf{V}_p\cdot\nabla_p\eta]<0$ (vorticity advection convergence—VAC) in this region and $\partial_t u_g<0$ will result, according to Eq. 1. The agreement between the Eulerian acceleration (Fig. 3) and VAC (Fig. 5) that is highlighted by the inclusion of $\partial_t u_g = -15\times10^6$ ms^{-2} (thick red dashed contour) and $\partial_t u_g = +15\times10^6$ ms^{-2} (thick blue dashed contour) in the latter, shows this. Furthermore there is vorticity advection divergence (VAD) north east of where $\partial_x^2 z=0$ in the eastern half of the COLs because vorticity advection increases there. This gives rise to $\partial_t u_g>0$.

These features are shown in Fig. 5, which begins from $t = -24$ h to $t = +36$ h. At t = – 24 h and – 12 h, in the vicinity of the COL closed circulation, the VAC decelerates the flow. This causes the split jet to form. The VAD north of that causes the small scale jet streak (see Sect. 3.1 and Ndarana and Waugh 2010) to form. Therefore the northward reduction of negative vorticity advection gives rise to the jet streak. Once the jet streak matures, the VAC and VAD fields move to the jet streak entrance and exit, respectively. This is influenced by the movement of the vorticity advection discussed above, which has to take place in order to move the COLs eastward. It may be concluded from this sequence of events that the sources and sinks of vorticity advection first establish the wind patterns near the COLs. Furthermore, recalling the $\partial_t u_g>0$ structure from the previous section that propagates north-easterly into the COL region; Fig. 5 shows that there is VAD associated with this process. Therefore the anticyclonic vorticity is advected into the closed circulation, which will act to off set the negative vorticity field there, thus acting to dissipate the COLs. This is a direct result of the negative vorticity advection field associated with undulations in the geopotential heights south-west of the COLs. Also consistent with Fig. 3, VAC and VAD contribute to the deceleration and acceleration of the midlatitude jet streak entrance and exit, which means that the eastward propagation of the vorticity field in the midlatitudes also affects the flow, south of the closed circulation.

Lastly, the effect of the meridional divergence of temperature advection appears to augment that of VAC in Eq. 1. However, the magnitude of the former is smaller compare the left and right panels of Fig. 5, meaning that the net effect of the terms on the right hand side is that the divergence of vorticity advection is the more dominant forcing on the Eulerian acceleration of the geostrophic zonal flow.

Impact of advective processes

The evident impact of VAC and VAD on the midlatitude jet is not sufficient to explain how the jet is propelled and how its orientation is altered. The reason for this way of thinking is that VAC and VAD are sinks and sources of vorticity advection, rather than propelling processes. It would be the vorticity advection itself that propels fields, but as it is well known, it moves the vorticity field and not the jet streams. In this section we consider zonal momentum advective processes as the possible mechanism that helps move the streak. We propose the use of the quasi-geostrophic momentum equation, given by

$$\partial_t u_g = -\mathbf{V}_p\cdot\nabla_p u_g + (f_o+\beta y)(v_g+v_a) - \partial_x\Phi \qquad (2)$$

for this purpose. Here v_a, β and Φ are the meridional ageostrophic wind, the beta effect and the geopontential. The last two terms of Eq. 2 are the Coriolis force and the zonal component of the pressure gradient force The former will tend to change the orientation of the flow whose zonal component is u_g towards the meridional direction, rather than its magnitude. It will therefore contribute little to propelling the jet stream eastward. It is also evident from Fig. 4 that where the midlatitude jet is located, $\partial_x \Phi \sim 0$ because the geopotential height fields are zonal there. It follows then that the important term in the region of the jet stream is the advection term ($-\mathbf{V}_g \cdot \nabla_p u_g$), which by definition is the transfer of zonal momentum by the geostrophic flow.

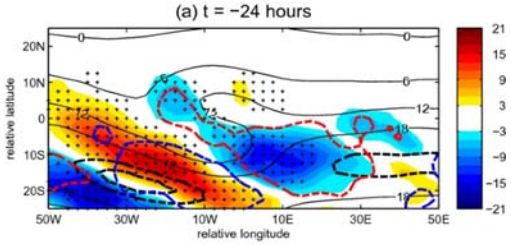
(a) t = −24 hours
relative latitude
relative longitude
20N
10N
0
10S
20S
50W
30W
10W
10E
30E
50E
21
15
9
3
−3
−9
−15
−21

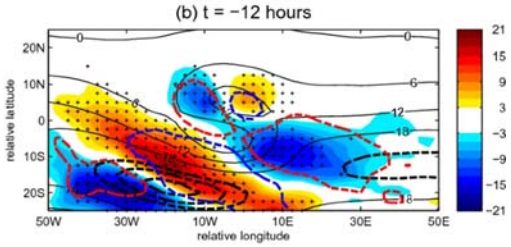
(b) t = −12 hours
relative latitude
relative longitude
20N
10N
0
10S
20S
50W
30W
10W
10E
30E
50E
21
15
9
3
−3
−9
−15
−21

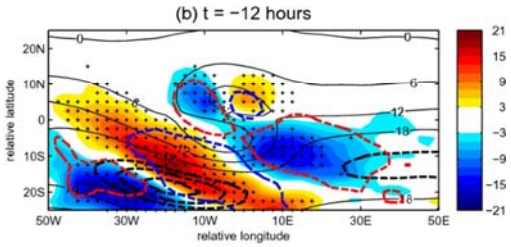
(b) t = −12 hours
relative latitude
relative longitude
20N
10N
0
10S
20S
50W
30W
10W
10E
30E
50E
21
15
9
3
−3
−9
−15
−21

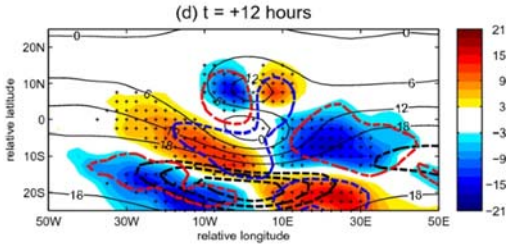
(d) t = +12 hours
relative latitude
relative longitude
20N
10N
0
10S
20S
50W
30W
10W
10E
30E
50E
21
15
9
3
−3
−9
−15
−21

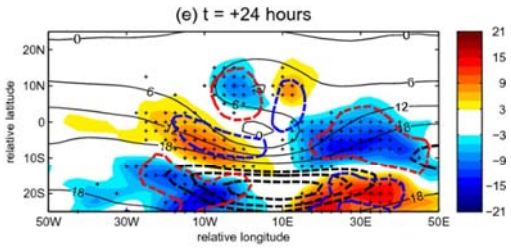
(e) t = +24 hours
relative latitude
relative longitude
20N
10N
0
10S
20S
50W
30W
10W
10E
30E
50E
21
15
9
3
−3
−9
−15
−21

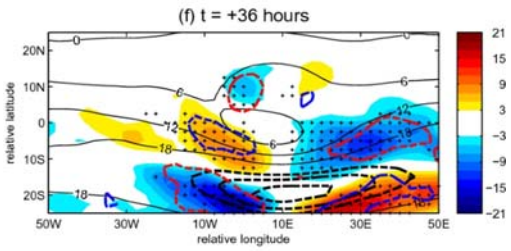
(f) t = +36 hours
relative latitude
relative longitude
20N
10N
0
10S
20S
50W
30W
10W
10E
30E
50E
21
15
9
3
−3
−9
−15
−21

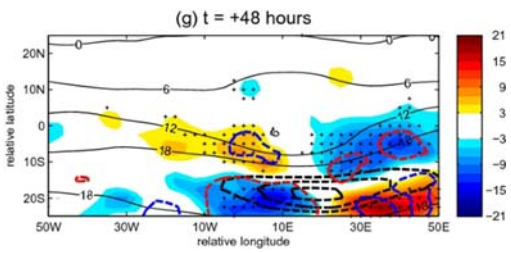
(g) t = +48 hours
relative latitude
relative longitude
20N
10N
0
10S
20S
50W
30W
10W
10E
30E
50E
21
15
9
3
−3
−9
−15
−21

Fig. 6. Time-lagged composites of 500 hPa $-u_g \partial_x u_g$, both plotted in 10^6 m^2 s^{-2}. The red (blues) thick dashed contours represent $-\mathbf{V}g \cdot \nabla pug = -6\ (+\ 6) \times 10^6$ m^2 s^{-2}. The black contours are the same as in Fig. 2. The crosses represent areas where the advection fields are significant at the 95% significance level. The composites are plotted from **a** t = – 24 h to **g** t = + 48 h, in 12 h intervals

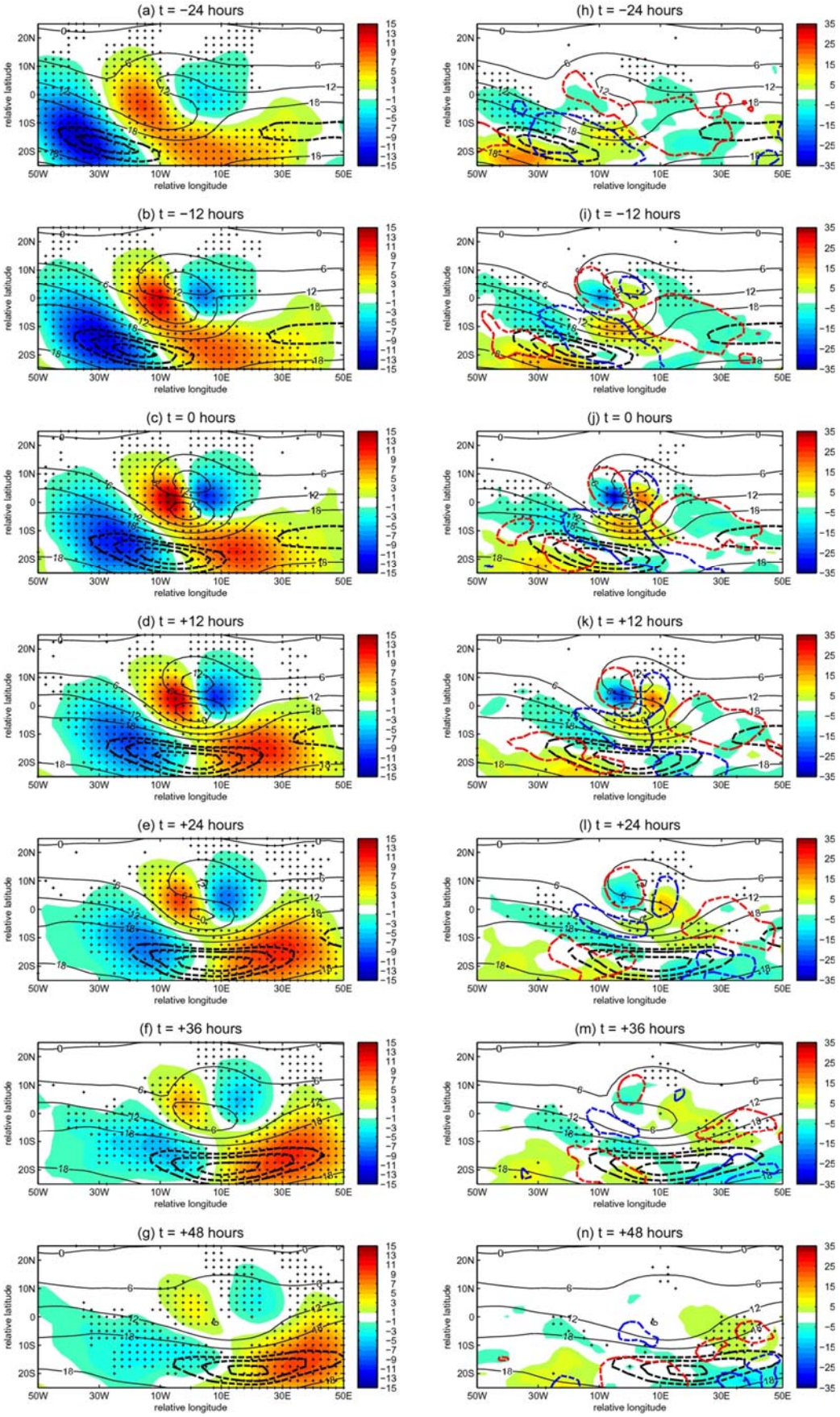
(a) t = −24 hours
(h) t = −24 hours
(b) t = −12 hours
(i) t = −12 hours
(c) t = 0 hours
(j) t = 0 hours
(d) t = +12 hours
(k) t = +12 hours
(e) t = +24 hours
(l) t = +24 hours
(f) t = +36 hours
(m) t = +36 hours
(g) t = +48 hours
(n) t = +48 hours
relative latitude
relative longitude
20N
10N
0
10S
20S
50W
30W
10W
10E
30E
50E

Fig. 7. Time-lagged composites of 500 hPa v_g (left panels) plotted in m s^{-1} and $-v_g\partial_y u_g$ (right panels) plotted in 10^6 m^2 s^{-2}. The red (blues) thick dashed contours represent $-\mathbf{V}g\cdot\nabla pug = -6\ (+6) \times 10^6$ m^2 s^{-2}. The black contours are the same as in Fig. 2. The crosses represent areas where v_g and $-v_g\partial_y u_g$ are significant at the 95% significance level. The composites are plotted from (**a**) t = − 24 h to (**g**) t = + 48 h, in 12 h intervals

For clarity of what their roles might be, we plot $-u_g\partial_x u_g$ (Fig. 6) and $-u_g\partial_x u_g$ (Fig. 7), separately, and superimpose $-\mathbf{V}_g\cdot\nabla_p u_g = -6\ (+6) \times 10^6$ m^2 s^{-2} represented by the thick dashed red (blue) contours. We discuss the advection of zonal momentum by the zonal flow in Fig. 6 first. Given the well known structure of jet streaks (Keyser and Shapiro 1985), $\partial_x u_g > 0$ at the entrance up to the point where the flow reaches a maximum within the streak and at the exit, $\partial_x u_g < 0$ because the jet strength decreases from the centre eastward. Since $u_g > 0$ within the jet streak, then the momentum advection ($-u_g\partial_x u_g$) is negative and positive at the entrance and exit, respectively. Since $-u_g\partial_x u_g > 0$ at time t at the jet exit transfers momentum eastward so the flow gains momentum downstream at time $t+1$, downstream of the jet streak. Therefore the jet looses momentum at the entrance. This shows that the zonal flow advects zonal momentum from the jet streak entrance to the exit, which propels the jet stream eastward. Figure 6 shows that this takes place on the poleward side of the jet streak axis, exactly where $\partial_t u_g < 0$, as indicated in Fig. 3. It appears from Fig. 6 that momentum is advected into the jet exit, where there is acceleration of the zonal flow. This suggests that the term $-u_g\partial_x u_g$ propels the midlatitude jet streak eastward, but does not account for the change in its orientation. This is a function of $-v_g\partial_y u_g$ presented in Fig. 7.

To motivate for the $-v_g\partial_y u_g$ pattern, we first consider the ambient meridional flow that is associated with COLs. This is shown in the left panels of Fig. 7. On the one hand, there exists poleward (equatorward) meridional geostrophic flow at the jet entrance (exit) which becomes weaker (stronger) as the jet translates eastward. The changes in the meridional flow filed indicate how they might influence the orientation of the jet streak during its evolution. These flow patterns inform those of meridional advection of zonal momentum (right panels of Fig. 7). Recalling that on the equatorward side of the jet, the barotropic shear is positive ($\partial_y u_g > 0$) and therefore $-v_g\partial_y u_g$ becomes negative at the equatorward entrance into the jet and positive at the equatorward exit. Similarly, $\partial_y u_g < 0$ on the poleward side of jet, so that the poleward entrance and exit are characterised by positive and negative values of meridional advection of zonal momentum, respectively. These patterns suggest that during the evolution of the jet streak and COLs, momentum transport is southward at the tail end of the streak and northward at its head. This changes the orientation of the streak from north-westerly/south-easterly, to easterly and then finally to south-westerly/north-easterly.

Concluding remarks

Using 39 years of ERA-Interim reanalysis data from 1979 to 2018, this study extended aspects of the results of Ndarana and Waugh (2010) and Reyers and Shao 415 (2019) in respect of the zonal wind flow that materialises during the evolution of COLs. It was shown in those studies that a small jet streak develops north of the COL closed circulation and that reduced and sometimes negative zonal flow develops within the closed circulation region. This jet streak is quasi-stationary. Furthermore a larger scale jet streak, located to the south-west of the COL centre, propagates eastward. As it does so PV associated with this evolution turns back on itself, such that $\partial_y P < 0$, P is PV. This signals RWB. The PV anomaly that is established breaks off, to induce the closed circulation (Hoskins et al. 1985). In this study, these characteristics of COLs and the associated flow were considered for the South African

domain, whilst Ndarana and Waugh (2010) considered COLs in the whole of the SH and Reyers and Shao (2019) found consistent results in COLs that occur just off the coast of the Atacama Desert. This is therefore a robust feature of these systems. It is also independent of season.

In this study the COL wind structure in Ndarana and Waugh (2010) and Reyers and Shao (2019) was confirmed using the geostrophic zonal wind. Because of the approach to compositing, it was also confirmed that RWB is a pre-existing atmospheric condition that leads to the PV anomalies, at least for most of the COL events, even though we did not quantify exactly what the percentage of the COLs this is the case for. The structure of the geostrophic vorticity advection, i.e. positive (negative) and a maximum (minimum) at the inflection point or line west (east) of the COL trough axis (Godoy et al. 2011), is similar to idealised situations (Holton and Hakim 2014) and support the use of the quasi-geostrophic framework in diagnosing the changes in the zonal winds. Given this structure, the advection is convergent across the axis of the COLs, which decelerates the zonal flow, by the u_g tendency equation. The formation of the split jet that Ndarana and Waugh (2010) as well as Reyers and Shao (2019) refer to is therefore caused by the convergence of vorticity advection. Vorticity advection diverges north of the COL and split jet formation causing the small scale jet streak to form. What this suggests is a feedback-like relationship between the zonal flow and the COLs in the vicinity of the closed circulation, i.e. COLs and the zonal flow immediately surrounding them influence each other.

Vorticity advection convergence and divergence also accelerate and decelerate the jet entrance and exits of the midlatitude jet, respectively. This is consistent with the movement of the jet in the northwesterly flow (Lang and Martin 2014) towards the base of the ridge, located south of the closed circulation of the COLs. As was the case with the small scale jet streak, the movement of the trough/ridge system in the middle latitudes plays a role in accelerating the jet streak.

The vorticity advection field does not explain the eastward propagation of the jets, but does suggest that eastward propagation of the troughs and ridges affect the flow, in keeping with wave-mean flow interaction theory (e.g. Edmon et al. 1980; Hoskins et al. 1983; Plumb 1986; Takaya and Nakamura 2001; Reviére and Orlanski 2007). These studies use different basic state flows, from zonally averaged to zonally varying low frequency ones. The eastward propagation and changes in the orientation of the jet is better explained from a momentum advection point of view. In the midlatitudes, where the zonal pressure gradients are relatively small, as compared to the regions where COLs form, the local acceleration of the jet is caused by the eastward advection of zonal momentum. The zonal flow advects zonal momentum from the jet entrance to the jet exit, and we propose that the midlatude jet is propelled eastward by this process. At the same time, its orientation is changed at it reaches the base of the midlatitude ridge (Keyser and Shapiro 1986; Lang and Martin 2012). This is caused by poleward (equatorward) acceleration of zonal momentum at the jet entrance (exit).

Causality between RWB and COLs remains unresolved. By addressing the dynamical processes that explain the evolution of the flow that is coupled to COL development and decay is an important component to this causality problem. An envisaged future task is to employ idealised simulations to test the hypothesis that RWB together with the flow structures explained in this study cause COLs. The immediate implications of the results obtained here together with those of the envisaged modelling study is an improvement in the medium range forecasting time scale predictability of COLs over South Africa. If these

results contribute to understanding dynamical processes that are associated with these systems, then they may potentially contribute to the development of medium range forecasting systems that could save lives.

Acknowledgements

The authors would like to thank Prof Darryn Waugh for commenting on the contents of the paper and the two anonymous reviewers who provided valuable constructive criticism of the paper.

Funding

This research was supported by Water Research Commission (Grant K5-2829).

References

Abatzoglou JT (2016) Contribution of cutoff lows to precipitation across the United States. J Appl Meteo Clim 55:893–899

Barnes MA, Ndarana T, Landman WA (2020) Cut-off lows in the southern Hemisphere and their extension to the surface. Clim Dyn (**submitted**)

Bell FG (1994) Floods and landslides in Natal and notably the Greater Durban Region, September 1987: a Retrospective view. Environ Eng Geosci XXXI:59–74

Bowley KA, Gyakum JR, Atallah EH (2019) A new perspective toward cataloging Northern Hemisphere Rossby Wave breaking on the dynamic Tropopause. Mon Wea Rev 147(409):431

Brown TJ, Hall BL (1999) The use of t values in climatological composite analyses. J Clim 12:2941–2944

Dee DP, Uppala SM, Simmons AJ, Berrisford P, Poli P, Kobayashi S, Andrae U, Balmaseda MA, Balsamo G, Bauer P, Bechtold P, Beljaars AC, van de Berg L, Bidlot J, Bormann N, Delsol C, Dragani R, Fuentes M, Geer AJ, Haimberger L, Healy SB, Hersbach H, Hlm EV, Isaksen L, Kllberg P, Khler M, Matricardi M, McNally AP, MongeSanz BM, Morcrette J, Park B, Peubey C, de Rosnay P, Tavolato C, Thpaut J, Vitart F (2011) The ERA Interim reanalysis: con guration and performance of the data assimilation system. Q J R Meteorol Soc 137:553–597

Dong L, Colucci SJ (2015) The role of non-quasigeostrophic forcing in Southern Hemisphere blocking onsets. Mon Weather Rev 143:1455–1471

Dyson L (2015) A heavy rainfall sounding climatology over Gauteng South Africa, using self-organising maps. Clim Dyn 45:3051–3065

Edmon HJ, Hoskins BJ, McIntyre ME (1980) Eliassen-Palm cross sections for the troposphere. J Atmos Sci 37:2600–2616

Favre A, Hewitson B, Lennard C, Cerezo-Mota R, Tadross M (2013) Cut-off lows in the South Africa region and their contribution to precipitation. Clim Dyn 41:2331–2351

Fuenzalida HA, Sánchez R, Garreaud RD (2005) A climatology of cutoff lows in the Southern Hemisphere. J Geophys Res Atmos 110:1–10

Gan MA, Piva E (2013) Energetics of a southeastern Pacific cut-off low. Atmos Sci Lett 14:272–280

Gan MA, Piva ED (2016) Energetics of southeastern Pacific cutoff lows. Clim Dyn 46:3453–3462

Godoy AA, Possia NE, Campetella CM, Skabar YG (2011) A cut-off low in southern South America; dynamic and thermodynamic processes. Revista Brasileira de Meteorologia 26:503–514

Holton JR, Hakim GJ (2013) An introduction to dynamic meteorology, 5th edn. Elsevier Academic Press, p 553

Holton JR, Hakim GJ (2014) An Introduction to Dynamic Meteorology. 5th edn. Elsevier Academic Press, p 553

Hoskins BJ, Mcintyre ME, Robertson AW (1985) On the use and significance of isentropic potential vorticity maps. Q J R Meteor Soc 111:877–946

Keyser D, Shapiro MA (1986) A review of the structure and dynamics of upper level frontal zones. Mon Wea Rev 114:452–499

Kunz T, Fraedrich K, Lunkeit F (2009) Response of idealized baroclinic wave life cycles to stratospheric flow conditions. J Atmos Sci 66:2288–2302

Kunkel D, Hoor P, Wirth V (2016) The tropopause inversion layer in baroclinic life-cycle experiments: the role of diabatic processes atmos. Chem Phys 16:541–560

Lang AA, Martin JE (2012) The structure and evolution of lower stratospheric frontal zones. Part 1: examples in northwesterly and southwesterly flow. Q J R Meteorol Soc 138:1350–1365

Martin JE (2014) Quasi-geostrophic diagnosis of the influence of vorticity advection on the development of upper level jet-front systems. Q J R Meteorol Soc 140:2658–2671

Nakamura M, Plumb RA (1994) The effects of flow asymmetry on the direction of Rossby wave breaking. J Atmos Sci 51:2031–2045

Ndarana T, Waugh DW (2010) The link between cut-off lows and Rossby wave breaking in the Southern Hemisphere. Q J R Meteor Soc 136:869–885

Ndarana T, Bopape M, Waugh D, Dyson D (2018) The Influence of the lower stratosphere on ridging Atlantic Ocean anticyclones over South Africa. J Clim 31:6175–6187

Ndarana T, Mpati S, Bopape M, Engelbrecht F, Chikoore H (2020) The flow and moisture fluxes associated with ridging South Atlantic Ocean anticyclones during the subtropical southern African summer. Submitted Int J Climatol

Nieto R et al (2005) Climatological features of cutoff low systems in the Northern Hemisphere. J Clim 18:3085–3103

Orlanski I, Katzfey J (1991) The life cycle of a cyclone wave in the Southern Hemisphere. 1. Eddy energy budget. J Atmos Sci 48:1972–1998

Orlanski I, Sheldon JP (1995) Stages in the energetics of baroclinic systems. Tellus 47A:605–628

Palmén E, Newtown CW (1979) Atmospheric circulation systems, their structure and physical interpretation. Academic Press, Cambridge

Pelmén E, Newtown CW (1969) Atmospheric circulation systems, their structure and physical interpretation. Academic Press

Peters D, Waugh DW (2003) Rossby wave breaking in the Southern Hemisphere wintertime upper troposphere. Mon Wea Rev 131:2623–2634

Pinheiro HR, Hodges KI, Gan MA, Ferreira NJ (2017) A new perspective of the climatological features of upper level cutoff lows in the Southern Hemisphere. Clim Dyn 48:541–559Pinheiro HR, Hodges KI, Gan MA (2019) Sensitivity of identifying cutoff lows in the Southern Hemisphere using multiple criteria: implications for numbers, seasonality and intensity. Clim Dyn 53:6699–6713

Plumb RA (1986) Three-dimensional propagation of transient quasi-geostrophic eddies and its relationship with the eddy forcing of the time-mean flow. J Atmos Sci 43:1657–1678

Porcù F, Carrassi A, Medaglia CM, Prodi F, Mugnai A (2007) A study on cut-off low vertical structure and precipitation in the Mediterranean region. Meteorol Atmos Phys 96:121–140

Price JD, Vaughan G (1993) The potential for stratosphere-troposphere exchange in cut-off low systems. Q J R Meteorol Soc 119:343–365

Pyle ME, Keyser D, Bosart LF (2004) A diagnostic study of jet streaks: kinematic signatures and relationship to coherent Tropopause disturbances. Mon Wea Rev 132:297–319

Reboita MS, Nieto R, Gimeno L, Da Rocha RP, Ambrizzi T, Garreaud R, Krger LF (2010) Climatological features of cutoff low systems in the Southern Hemisphere. J Geophys Res Atmos 115:D17104

Reyers M, Shao Y (2019) Cut off lows off the coast of the Atacama Desert under present day condition and in the Last Glacial Maximum. Global Planet Change 181:102–983

Riviére G, Orlanski I (2007) Characteristics of the Atlantic storm track eddy activity and its relation with the North Atlantic Oscillation. J Atmos Sci 64:241–266

Shapiro MA (1982) Mesoscale weather systems of the central United States. CIRES Univ. of Colorado/NOAA, Boulder, p 78

Singleton AT, Reason CJC (2006) A numerical model study of an intense cut-off low pressure system over South Africa. Mon Wea Rev 135:1128–1150

Singleton AT, Reason CJC (2007) Variability in the characteristics of cut-off low pressure systems over subtropical Southern Africa. Int J Climatol 27:295–310

Stander JH, Dyson L, Engelbrecht CJ (2016) A snow forecasting decision tree for significant snowfall over the interior of South Africa. S Afr J Sci 112(9/10):1–10

Takaya K, Nakamura H (2001) A formulation of a phase-independent wave-activity flux for stationary and migratory quasigeostrophic eddies on a zonally varying basic flow. J Atmos Sci 58:608–627

Tennant W (2004) Considerations when using pre-1979 NCEP/NCAR reanalysis in the southern hemisphere. Geophys Res Lett 31:L11112

Thorncroft CD, Hoskins BJ, McIntyre ME (1993) Two paradigms of baroclinic-wave life-cycle behaviour. Q J R Meteor Soc 119:17–55

Wang S, Polvani LM (2011) Double tropopause formation in idealized baroclinic life cycles: the key role of an initial tropopause inversion layer. J Geophys Res 116:D05108

Waugh DW, Polvani LM (2000) Climatology of intrusions into the tropical upper troposphere. Geophys Res Lett 27:3857–3860